Refined structure of monomeric diphtheria toxin at 2.3 Å resolution

M.J. BENNETT AND DAVID EISENBERG

Molecular Biology Institute, Department of Chemistry and Biochemistry, and UCLA-DOE Laboratory of Structural
Biology and Molecular Medicine, University of California at Los Angeles, Los Angeles, California 90024-1570

Abstract

The structure of toxic monomeric diphtheria toxin (DT) was determined at 2.3 Å resolution by molecular replacement based on the domain structures in dimeric DT and refined to an R factor of 20.7%. The model consists of 2 monomers in the asymmetric unit (1,046 amino acid residues), including 2 bound adenylyl 3'-5' uridine 3' monophosphate molecules and 396 water molecules. The structures of the 3 domains are virtually identical in monomeric and dimeric DT; however, monomeric DT is compact and globular as compared to the "open" monomer within dimeric DT (Bennett MJ, Choe S, Eisenberg D, 1994b, *Protein Sci 3*:0000-0000). Detailed differences between monomeric and dimeric DT are described, particularly (1) changes in main-chain conformations of 8 residues acting as a hinge to "open" or "close" the receptor-binding (R) domain, and (2) a possible receptor-docking site, a β-hairpin loop protruding from the R domain containing residues that bind the cell-surface DT receptor. Based on the monomeric and dimeric DT crystal structures we have determined and the solution studies of others, we present a 5-step structure-based mechanism of intoxication: (1) proteolysis of a disulfide-linked surface loop (residues 186-201) between the catalytic (C) and transmembrane (T) domains; (2) binding of a β-hairpin loop protruding from the R domain to the DT receptor, leading to receptor-mediated endocytosis; (3) low pH-triggered open monomer formation and exposure of apolar surfaces in the T domain, which insert into the endosomal membrane; (4) translocation of the C domain into the cytosol; and (5) catalysis by the C domain of ADP-ribosylation of elongation factor 2.

Keywords: ADP-ribosyltransferase; diphtheria; membrane insertion; receptor recognition

Diphtheria toxin (DT) is a 535-residue protein that causes the disease diphtheria. DT is secreted from toxic strains of the bacterium *Corynebacterium diphtheriae* lysogenized with a phage carrying the DT gene (Freeman, 1951). DT has 3 functions during cell intoxication, which are performed by folding domains (C, catalytic; T, transmembrane; R, receptor-binding) (Choe et al., 1992). The R domain binds to a cell-surface receptor and DT is endocytosed from coated pits (Morris et al., 1985). Within the low pH of the endosome, DT undergoes a conformational change and inserts into the endosomal membrane (London, 1992). The C domain is then translocated across the membrane, into the cytosol, where it catalyzes the transfer of ADP-ribose from NAD to elongation factor 2 (EF-2), halting protein synthesis and killing the cell (Collier, 1975).

To illuminate the structural basis of this process of intoxication, it was essential to determine the structure of the toxic monomeric form of DT. Also, the 2.0-Å resolution structure of

nontoxic dimeric DT revealed that the monomer within dimeric DT has an open structure unlike most globular proteins (Bennett et al., 1994b [companion paper]), and it was essential to determine how the monomeric and dimeric DT structures differ. From the structures of both monomeric and dimeric DT, we have been able to infer some aspects of the structural basis of DT intoxication.

Results

Overall refined monomeric DT structure

The monomeric DT model is refined to a crystallographic R factor of 20.7% based on 42,844 reflections ($F > 1\sigma(F)$) between 10 and 2.3 Å resolution. Statistics for assessing the quality of the monomeric DT model are listed in Table 1. The 2 monomers in the asymmetric unit were refined independently; the model consists of 8,042 non-hydrogen protein atoms, 86 dinucleotide (ApUp, adenylyl 3'-5' uridine 3' monophosphate) atoms, and 396 water molecules. As in the dimeric DT model, a flexible loop between the C and T domains (residues 188-199) is not included

Table 1. *Quality of the monomeric DT model refined at 2.3 Å with XPLOR*

Crystallographic R factor (%)	20.7
Number of reflections ($F > 1\sigma(F)$)	42,844
Resolution range (Å)	10.0–2.3
Completeness (%)	88.8
RMS deviations from target geometry	
Bond lengths (Å)	0.022
Bond angles (deg)	2.4
Dihedral angles (deg)	25.8
Improper angles (deg)	2.0
Number of non-hydrogen atoms	
Protein (2 DT monomers)	8,042
Dinucleotide (2 ApUp)	86
Water	396
Total	8,524
Average overall B factor (Å^2)	20

in the monomeric DT model because of disorder. To distinguish between the 2 monomers in the asymmetric unit, residues 1–535 refer to residues in monomer "1," placed in the unit cell according to the top solutions to the rotation and translation functions (see Materials and methods). Residues 1'–535' refer to monomer "2," related by noncrystallographic 2-fold symmetry.

Figure 1 is a plot of the RMS differences between Cα positions in the 2 monomers in the asymmetric unit after superposition of Cα atoms differing by <2 Å. The overall RMS difference is 0.4 Å; if 5 residues differing by >1 Å (labeled in Fig. 1) are excluded, the difference is 0.3 Å. Labeled residues in Figure 1 are: residues 350–353 in a poorly defined loop that has high main-chain temperature (B) factors and is modeled dif-

ferently in the 2 monomers in the asymmetric unit, and residue 498 in a disordered surface loop. The noncrystallographic 2-fold symmetry is preserved for 119 water molecules with equivalent positions within 1 Å in each monomer. The overall RMS difference for these 119 pairs of water molecules is 0.5 Å.

Structural similarity of monomeric and dimeric DT

A stereo figure of monomeric DT is shown in Figure 2 (see Kinemage 2). The 3 domains are labeled C (catalytic, upper left), T (transmembrane, bottom), and R (receptor-binding, upper right). The structure of each of the 3 folding domains is virtually identical to that found in dimeric DT, with the exception of residues in crystal contacts and residues in the hinge loop (residues 379–386), which permits the large movement of the R domain discussed below. The interfaces between domains in monomeric and dimeric DT are very similar in the amounts of buried surface areas (Richmond & Richards, 1978), hydrophobic folding energies estimated using atomic solvation parameters (Eisenberg & McLachlan, 1986), and polar interactions. One difference from the interdomain polar interactions found in dimeric DT (Bennett et al., 1994b) is that salt bridges involving Arg 173 in the C–T interface are not found in monomeric DT because the side chain of Arg 173 is in a different position, forming a crystal contact.

Figure 3 shows the DSSP (Kabsch & Sander, 1983) secondary structure assignments in dimeric DT compared to monomeric DT. The assigned secondary structures in monomeric DT are essentially the same as in dimeric DT, however, there are 2 differences requiring further comment. Residues in the hinge loop (residues 379–386) have a coil conformation in monomeric DT, whereas residues 381–387 form 2 consecutive reverse turns in dimeric DT (Kinemage 3). In addition, residues 517–518 and 521–522 extend the last 2 β-strands in the R domain and residues 519–520 form a type I' reverse turn stabilized by crystal
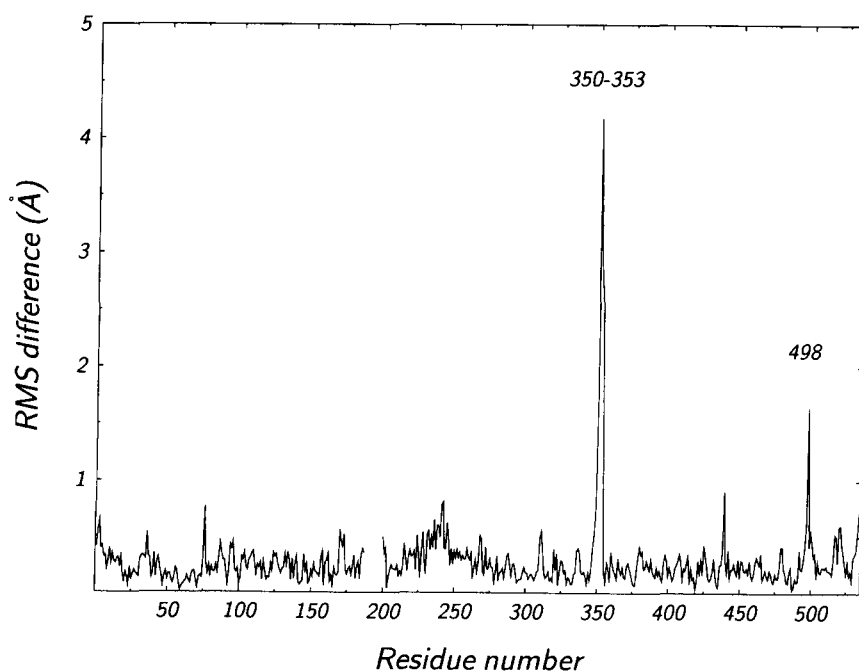

Fig. 1. Comparison of the 2 monomers in the asymmetric unit of monomeric DT crystals. RMS differences between Cα atoms are plotted against residue number and residues with RMS differences >1 Å are labeled. Excluding residues 350–353, which are modeled differently in the 2 monomers, and residue 498 in a surface loop, the overall RMS difference is 0.3 Å. RMS differences were calculated using the program OVERLAY (Kabsch, 1978) with a 2-Å cutoff.
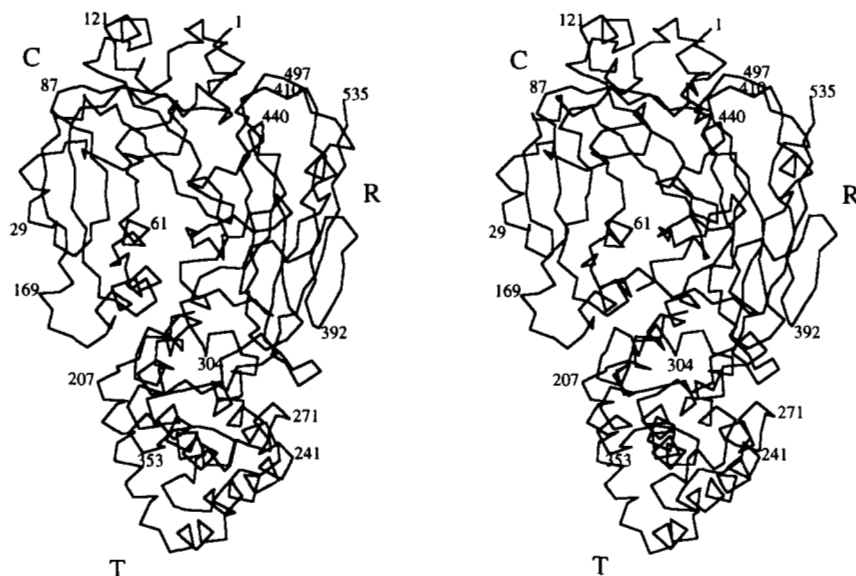
Fig. 2. Stereo figure of the Cα atoms of monomeric DT. Residues 188–199, in a disordered loop connecting the C and T domains, are not included in the model. The domains are indicated by the letters C (catalytic), T (transmembrane), and R (receptor-binding). Some residues are labeled for identification.

```
1      GADDVVDSSK SFVMENFSSY HGTKPGYVDS IQKGIQKPKS GTQGNYDDDW
D      GGGTB GGG  EEEET_EEE EEE TT TTG GGG             SS S TT SSGGG
M1     GGGTEEEEE  EEEEET_EEE EEE TTTTTG GGG            SS S TT SSGGG
          CB1       CB2           CH2

51     KGFYSTDNKY DAAGYSVDNE NPLSGKAGGV VKVTYPGLTK VLALKVDNAE
D      SEEEES HH  HHGGG B TT STTTS B  EE EEEE SSEEE EEEBS    HH
M1     SEEEES HH  HHHTT B TT STTTS B  EE EEEE SSEEE EEEES    HH
          CB3   CH3'                     CB4    CB5

101    TIKKELGLSL TEPLMEQVGT EEFIKRFGDG ASRVVLSLPF AEGSSSVEYI
D      HHHHHTT   S  SS HHHHHTS HHHHHHHSTT SEEEEEE     TT   EEEE
M1     HHHHHTT   S  SS HHHHHTTS HHHHHHHSTT SEEEEEEE    TT   EEEE
          CH4      CH4'       CH5         CB6          CB7

151    NNWEQAKALS VELEINFETR GKRGQDAMYE YMAQACAGNR VRRSVGSSLS
D      E TTGGGG E EEEEEEESGGG    STTHHHHHH HHGGGG *** *********
M1     E TTGGGG E EEEEEEESGGG    STTHHHHHH HHHGGG *** *********
          CH5'   CB8              CH7

201    CINLDWDVIR DKTKTKIESL KEHGPIKNKM SESPNKTVSE EKAKQYLEEF
D      HHHHH HHHHHHHHHH HH HHHHHHH HHS  S    H HHHHHHHHHH
M1     HHHHH HHHHHHHHHH HT HHHHHHH HTS  S    H HHHHHHHHHH
          TH1        TH2              TH3

251    HQTALEHPEL SELKTVTGTN PVFAGANYAA WAVNVAQVID SETADNLEKT
D      HHHHHTTSGGG HHHHHHTSS GGGSHHHHHH HHHHHHTT HHHHT HHHH
M1     HHHHHTTSGGG HHHHHHHHTT GGG HHHHHH HHHHHHHHH HHHHT HHHH
          TH4        TH5                 TH5'   TH6

301    TAALSILPGI GSVMGIADGA VHHNTEEIVA QSIALSSLMV AQAIPLVGEL
D      HHHHHTT  S  H HHHHTEETTE  E      SHHHHH HHHHHHHHHHH HHHHHHH   S
M1     HHHHHTT  S  H HHHHTEETTE  E      SHHHHH HHHHHHHHHH HHHHHHHS S
          TH7                TH8

351    VDIGFAAYNF VESIINLFQV VHNSYNRPAY SPGHKTQPFL HDGYAVSWNT
D      HHHHHHTHH HHHHHHHHHH HHHHHHS    TTSTT EE ETTEEEEESS
M1     HHHHHHTHH HHHHHHHHHH HHHHHTS    S SS EE ETTEEEEESS
          TH9                          RB1     RB2

401    VEDSIIRTGF QGESGHDIKI TAENTPLPIA GVLLPTIPGK LDVNKSKTHI
D      TGGGEEE_SS SEEEEEEEEE EESSS EEE  EEEEE BTTT BEE_TTT EE
M1     SGGGEEETT  SEEEEEEEEE EESSS EEE  EEEEE BTTT EEE TTT EE
          RB2'      RB3        RB3'   RB4      RB4'     RB5

451    SVNGRKIRMR CRAIDGDVTF CRPKSPVYVG NGVHANLHVA FHRSSSEKIH
D      EETTEEEEEE EEE SSSEEE EEESS EEEB TTB EEEEEE EEES  S
M1     EETTEEE EE EEEETTTEEE EEESS EEEB TTB EEEEEE EEE  SS
          RB6       RB7        RB7'      RB8

501    SNEISSDSIG VLGYQKTVDH TKVNSKLSLF FEIKS
D      TTT   SEEE EEEEEE GGG S EEEEEEEE  EEE
M1     TTT S EEE EEEEEEEETT EEEEEEEEEE  EEE
          RB9        RB10
```

Fig. 3. Comparison of secondary structure assignments in monomeric and dimeric DT. Upper line, amino acid sequence (Greenfield et al., 1983); second line, DSSP secondary structure assignments for the 2.0-Å refined dimeric DT model (Bennett et al., 1994b) (**D**) using the nomenclature of Kabsch and Sander (1983): E, β-strand; H, α-helix; G, 3_{10}-helix; B, isolated β-bridge; S, bend; T, hydrogen bonded turn; third line, DSSP secondary structure assignments for monomer 1 (**M1**) of the monomeric DT model. The secondary structure content of monomer 2 is virtually identical to that of monomer 1; fourth line, assignments of α-helices and β-strands (underlined) for monomeric and dimeric DT using a 3-character code referring to (1) the domain (C, catalytic; T, transmembrane; R, receptor-binding), (2) the secondary structure element (H, helix; B, β-strand), and (3) the number of sequential occurrences of each type of secondary structure within each domain. Asterisks indicate residues not included in the model because of disorder (residues 188–199). Residues in dimeric DT were visually inspected and assigned to secondary structures as described (Bennett et al., 1994b). Residues in monomeric DT were assigned to secondary structures using the same criteria. Four residues with similar φ and ψ angles to those in the dimer and without large RMS differences (residues 29, 64–66) were assigned to the same secondary structure as in the dimer, although the angles at donor and acceptor atoms deviated up to 12° from the cutoff value of 110°.

contacts in monomeric DT (discussed below), whereas residues 517-522 are disordered in dimeric DT.

Figure 4A is a plot of RMS differences between Cα positions in the 3 domains in monomeric and dimeric DT after superposing Cα atoms differing by <2 Å. The overall RMS differences for all Cα atoms in the C, T, and R domains are 0.4 Å, 1.4 Å, and 1.2 Å, respectively. If the residues with RMS differences >2 Å are excluded (labeled in Fig. 4A), the overall RMS differences for the T and R domains drop to 0.5 Å (based on 176 of 187 Cα atoms) and 0.8 Å (based on 136 of 149 Cα atoms), respectively. Excluding residues 380-387, in and near the hinge

loop (discussed below), and residues 408-411, near different crystal contacts in monomeric and dimeric DT, residues with RMS differences >2 Å (labeled in Fig. 4A) are in surface loops that are poorly defined in the electron density and have high main-chain *B* factors. Residues 40, 269, 438-439, and 498-503 are in or near intermolecular contacts in dimeric but not in monomeric DT crystals; the loss of these contacts may cause increased mobility and positional shifts in monomeric DT. The 3D-1D profile scores of monomeric and dimeric DT are compared in Figure 4B. The greatest differences are in the hinge loop (residues 379-386), which has higher profile scores in monomeric
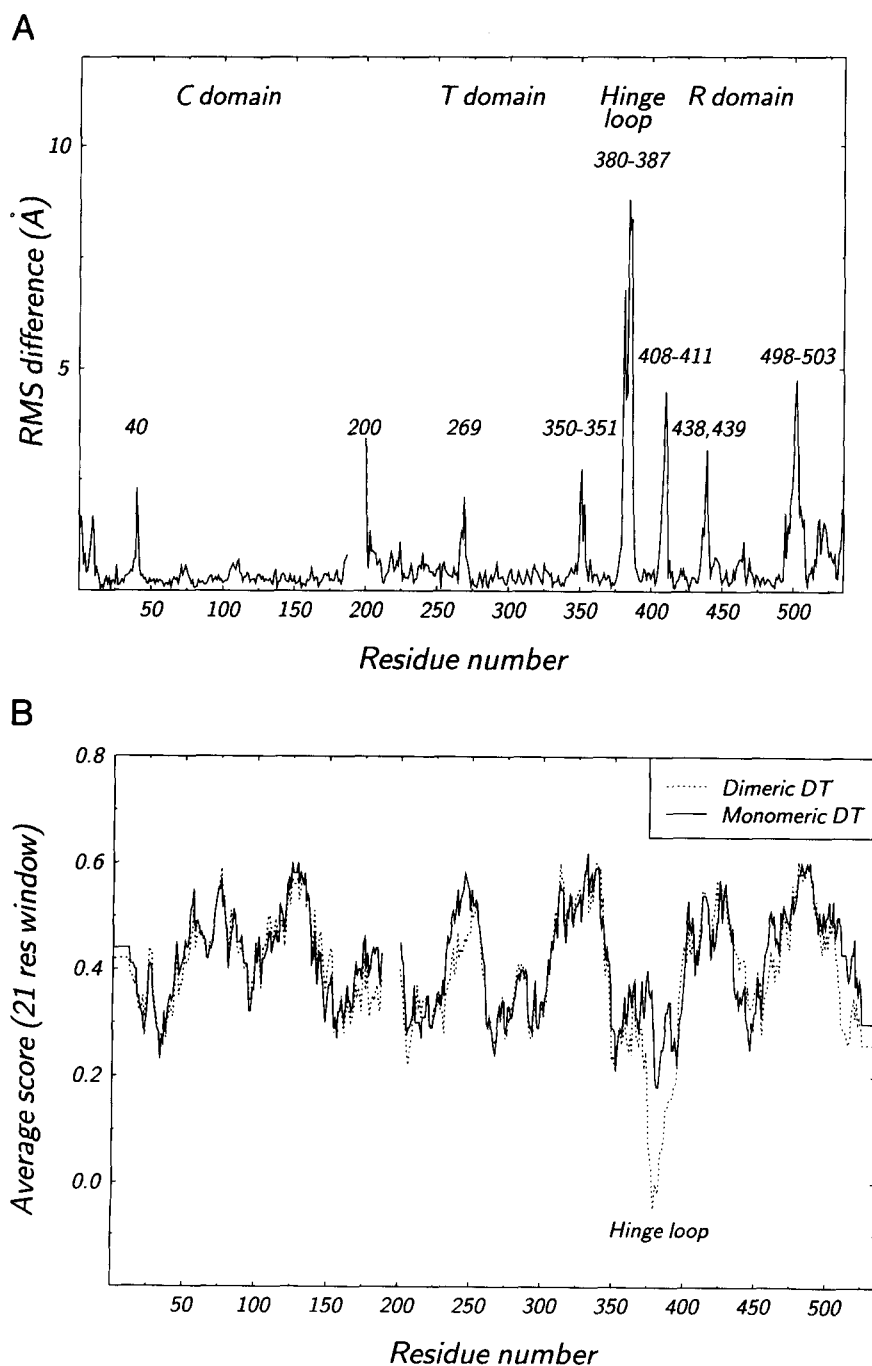

Fig. 4. Comparison of the monomeric and dimeric DT structures. **A:** RMS differences between Cα atoms in the 3 domains in monomeric and dimeric DT. The 3 domains and the hinge loop, which changes conformation upon dimerization (residues 379-386), are indicated. The RMS differences were calculated after superposition of Cα atoms using the program OVERLAY (Kabsch, 1978) with a 2-Å cutoff. Cα atoms in 3 domains of monomeric DT (monomer 1) and dimeric DT (residues 1-187, 200-386, and 387-535) were superposed separately. The overall RMS differences for the C, T, and R domains are 0.4 Å, 1.4 Å, and 1.2 Å, respectively. All residues with RMS differences >2 Å are labeled. If these residues are excluded, the overall RMS differences in the T and R domains drop to 0.5 Å and 0.8 Å, respectively. **B:** 3D-1D profile window plot: monomeric versus dimeric DT. The 3D-1D profile score (Bowie et al., 1991; Zhang & Eisenberg, 1994) is averaged over a 21-residue window and plotted versus residue number for the monomeric DT model (solid lines) and the 2.0-Å refined dimeric DT model (broken lines). The hinge loop (residues 379-386) is labeled.

DT. The hinge loop is the only segment that differs significantly between monomeric and dimeric DT (Fig. 4A and discussed below). Its higher profile scores in monomeric DT, reflecting greater compatibility of residues with their environments, are consistent with the greater stability of monomeric DT relative to domain-swapped dimeric DT (Carroll et al., 1986a; Bennett et al., 1994a).

There are differences in the toxicity of monomeric and dimeric DT: monomeric DT is toxic to animals and cultured cells, but dimeric DT is not (Carroll et al., 1986a). In addition, the DT crystal structures show that the active site in domain-swapped dimeric DT is formed by 2 subunits (Bennett et al., 1994b), whereas in monomeric DT, it is formed by 1 polypeptide chain. Because of these differences in toxicity and active-site composition, it is of interest to compare the active sites in monomeric and dimeric DT. The superposition of ApUp atoms and all atoms in residues within 5 Å of ApUp in monomeric and dimeric DT yields an overall RMS difference of 0.5 Å, indicating the active sites are very similar.

Structural differences between monomeric and dimeric DT: Hinge loop (residues 379–386)

The segment in Figure 4A with the largest RMS differences between Cα positions in monomeric and dimeric DT is the hinge loop between the T and R domains (residues 379–386). Changes in the positions of these 8 residues result in a large shift in the overall position of the R domain, although the structure of the R domain itself remains essentially unchanged. Figure 5A shows a comparison of the Cα backbones of the R domains of monomeric and dimeric DT, viewed approximately from the "back" of Figure 2.

The large movement of the entire R domain from monomeric to dimeric DT, shown in Figure 5A, is accomplished by changes in the main-chain torsion angles of residues 379–386. Table 2 shows a comparison between the main-chain torsion angles ϕ and ψ for these 8 residues and 2 flanking residues in the monomeric and dimeric DT models. Changing only the main-chain torsion angles of either Thr 386 or Lys 385 is sufficient to rotate the R domain into approximately its position in dimeric DT, swung away from the rest of the molecule. In other words, the main-chain atoms of Thr 386 or Lys 385 act as a molecular hinge. Upon dimerization by domain swapping, the main-chain conformations of other hinge loop residues may adjust to avoid steric clashes.

The side-chain conformations of His 484 and Lys 419 in the R domain are also affected by conformational changes in the hinge loop upon dimerization. In monomeric DT, the hinge loop crosses the back of the R domain like a strap across the β-sheet, whereas in dimeric DT the hinge loop is more exposed (Fig. 5A). In dimeric DT, His 484 is rotated 90° about χ_1 relative to its position in monomeric DT, filling a pocket occupied by the main-chain and side-chain atoms of Tyr 380 in the hinge loop in monomeric DT. Comparison of Figure 5B and C (structures overlaid in Kinemage 3) shows the differences in the position of Tyr 380: in monomeric DT, its side chain is packed against the R domain; in dimeric DT, it is more exposed. Similarly, in dimeric DT, the side chain of Lys 419 fills a pocket occupied by the main-chain atoms of residues 383–385 in the hinge loop in monomeric DT. Differences in the main-chain positions of residues 383–385 can be seen by comparing Figure 5B and C. The

Table 2. *Comparison of main-chain torsion angles of residues in and near the hinge loop[a] in monomeric and dimeric DT*

Residue	Monomeric DT[b]			Dimeric DT	
	ϕ (deg)	ψ (deg)	Distance[c] (deg)	ϕ (deg)	ψ (deg)
Pro 378	−66	127	8	−62	134
Ala 379	−63	122	99	−154	162
Tyr 380	−64	124	36	−99	131
Ser 381	−12	98	94	−74	169
Pro 382	−58	−38	173	−60	135
Gly 383	−66	142	158	85	8
His 384	−83	132	28	−109	141
Lys 385	−88	−15	173	47	−123
Thr 386	−132	162	148	−103	17
Gln 387	−58	124	15	−72	129

[a] The hinge loop (residues 379–386) connects the T and R domains and is the feature that differs most between monomeric and dimeric DT, as shown in Figure 4A.

[b] Torsion angles in monomer 1. Torsion angles in monomer 2 differ by less than 15°. Average difference between hinge loop torsion angles in the 2 molecules in the asymmetric unit is 5°

[c] Distance calculated as $(\Delta\phi^2 + \Delta\psi^2)^{1/2}$.

change in environments of residues 380, 384, and 385 contribute to the lower profile scores of the hinge loop in dimeric DT. In addition, the different side-chain positions of His 484 and Lys 419 allow the formation of different hydrogen bonds between the hinge loop and the R domain in monomeric DT or between the hinge loop and the symmetry-related R domain in dimeric DT.

Structural differences between monomeric and dimeric DT: Receptor-binding loop (residues 514–525)

The R domain of DT can be described as a flattened barrel of 10 antiparallel β-strands with a jellyroll fold (Richardson, 1981). Although the immunoglobulin (Ig) fold is distinct from the jellyroll fold, the Ig variable domain shares some topological features with the R domain of DT (Choe et al., 1992). The connection between the last 2 β-strands in the R domain (residues 514–525) is a protruding β-hairpin loop (Fig. 6) containing a residue necessary for receptor binding (Greenfield et al., 1987). Consistent with a role in molecular recognition, this protruding β-hairpin loop corresponds to CDR3 in the Ig variable domain, one of the hypervariable antigen-binding loops.

The 12-residue loop 514–525 (see Kinemage 2) may be regarded as a distinct substructure because residue 513 is the last residue that forms hydrogen bonds with a neighboring strand. Within the loop, residues 519 and 520 form a type I' reverse turn, which is stabilized by a salt bridge between Asp 519 and Lys 445' of a symmetry-related molecule (discussed below). Because of this crystal contact, the tip of the β-hairpin loop (residues 517–523) is well defined in the monomeric DT electron density maps, with lower B factors than in dimeric DT. In dimeric DT, the hydrogen bonds between residues 517 and 522 are disrupted, effectively decreasing the lengths of the last 2 β-strands in the R domain (Fig. 3).
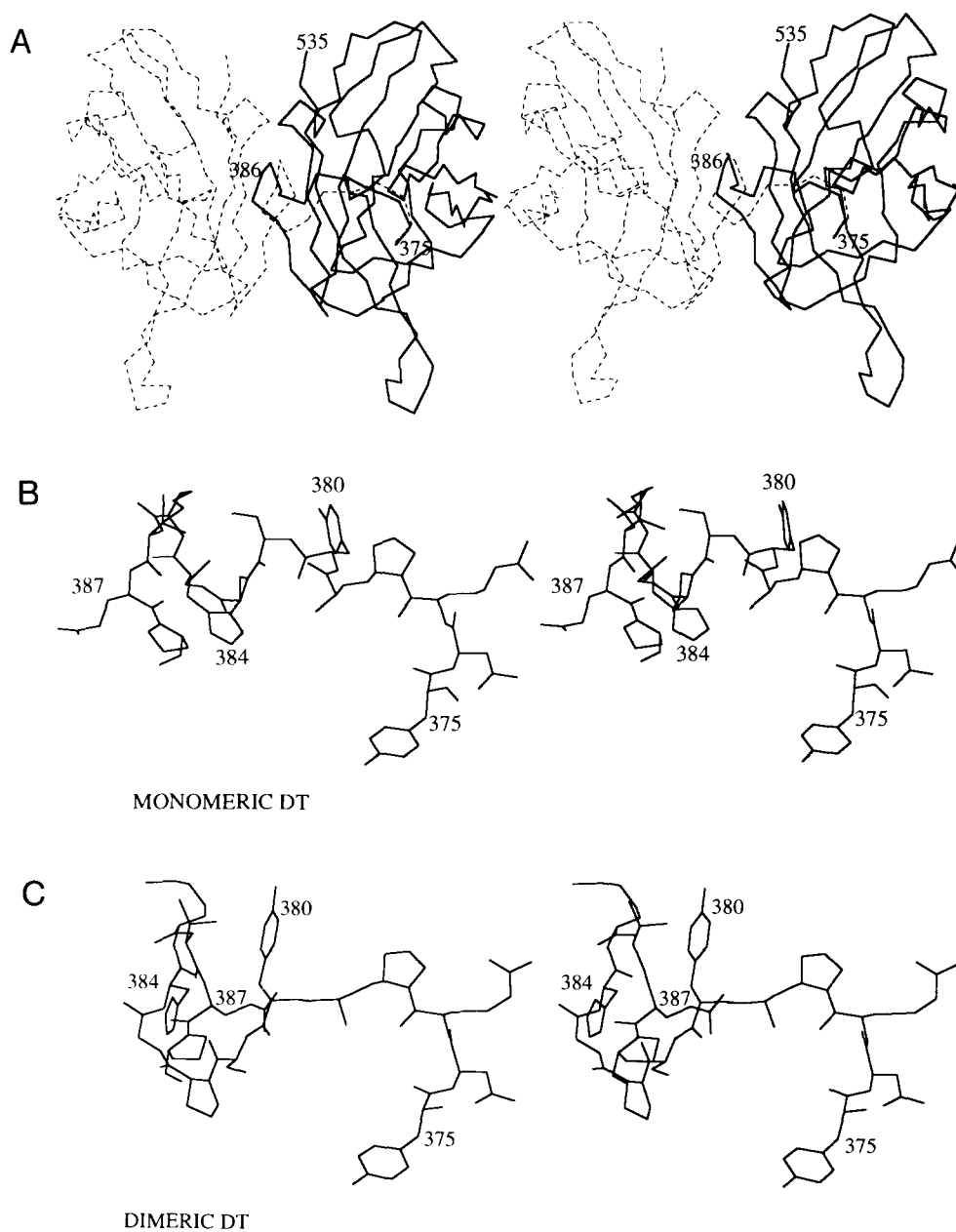
Fig. 5. The vast movement of the R domain upon dimerization. **A:** Stereo figure of Cα atoms in the R domains of monomeric and dimeric DT. The orientation is from the "back" of the monomeric model shown in Figure 2. Cα atoms in dimeric and monomeric DT are connected with broken and solid lines, respectively. Labels indicate residues in monomeric DT. Residues 375 and 386 are the approximate boundaries of the hinge loop and residue 535 is the carboxy-terminus of DT. Monomeric (monomer 1) and dimeric DT models were superimposed by least-squares fitting the Cα atoms of the C and T domains (residues 1-187 and 200-375) using XPLOR (Brünger et al., 1990), giving an overall RMS difference of 0.6 Å. **B:** Stereo figure of non-hydrogen atoms in or near the hinge loop in monomeric DT (residues 375-387). The orientation is the same as in A. **C:** Stereo figure of non-hydrogen atoms in or near the hinge loop in dimeric DT (residues 375-387). The orientation is the same as in A and B.

Intermolecular contacts within the asymmetric unit

Intermolecular contacts between 2 monomers related by non-crystallographic 2-fold symmetry are formed by residues in the first β-strand in each molecule (residues 12-15). These β-strands are antiparallel, with 2 half hydrogen bonds between the main-chain atoms of Val 13 in each molecule (denoted residues 13 and 13′) (Fig. 7). Three strands from each molecule (residues 12–

15, 88-94, 133-139) form a 6-stranded β-sheet across the non-crystallographic 2-fold axis.

This 2-fold axis between DT monomers at their C domains is distinct from the 2-fold axis that relates the monomers in dimeric DT at their R domains (Bennett et al., 1994b). The solvent-accessible surface area buried at this C domain contact was calculated (Richmond & Richards, 1978) and found to be about 400 Å² per subunit, which is less than is found in stable
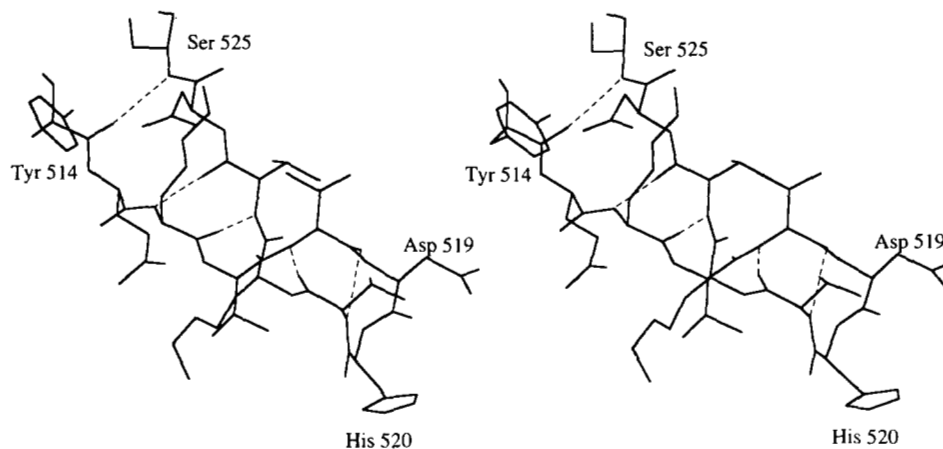
Fig. 6. Stereo figure of the receptor-binding loop of DT. All non-hydrogen atoms of residues 514–525 are shown. The 12 residues form a β-hairpin loop, which protrudes from the surface of the R domain. A salt bridge between Asp 519 and Lys 445′ of a symmetry-related molecule stabilizes the reverse β-turn at residues 519 and 520 in monomeric DT, whereas it is disordered in dimeric DT. Residue 525 (Greenfield et al., 1987) is known to be involved in receptor binding.

dimers (Janin et al., 1988). We do not expect that the dimer found within the asymmetric unit of monomeric crystals forms in solution because DT dimers of any sort are not formed at high monomer concentrations (30 mg/mL) (Carroll et al., 1986a).

Intermolecular crystal packing contacts and crystal morphology

Table 3 lists polar interactions between 2 DT monomers in the asymmetric unit and neighboring monomers in the crystal. In the following we note that the number of polar contacts in axial directions in the monomeric DT crystals is related to the crystal growth rate and morphology.

Table 3 shows that contacts between molecules related by translation along *c* (I) are the most abundant intermolecular interactions. There are also many intermolecular contacts in the *a* direction, between molecules related by the 2-fold screw axis along *a* (III). The contacts between monomers related by III include residues in the protruding β-hairpin loop in the R domain.

In contrast, there are only 2 intermolecular contacts in the *b* direction, between molecules related by the 2-fold screw axis along *b* (II). Unlike the interactions between molecules related by I and III, the contacts between molecules related by II are not duplicated in both monomers in the asymmetric unit.

The number of polar contacts in each axial direction can be correlated with the extent and rate of crystal growth in that direction: the longest dimension of the crystals is parallel to the *c* axis, the axis with the most intermolecular contacts; the shortest dimension is parallel to the *b* axis, the axis with the least contacts. Crystal macroseeds grow rapidly in the dimension parallel to the *c* axis, which initially leaves the crystals hollow at the ends because growth in the other 2 dimensions is slower (see Materials and methods).

Consistent with the similar intermolecular contacts in the 2 monomers in the asymmetric unit, *B* factors are virtually identical in the 2 monomers (not shown). The only exceptions are residues 222–260, which have lower *B* factors in monomer 2, perhaps because they are in different environments than the
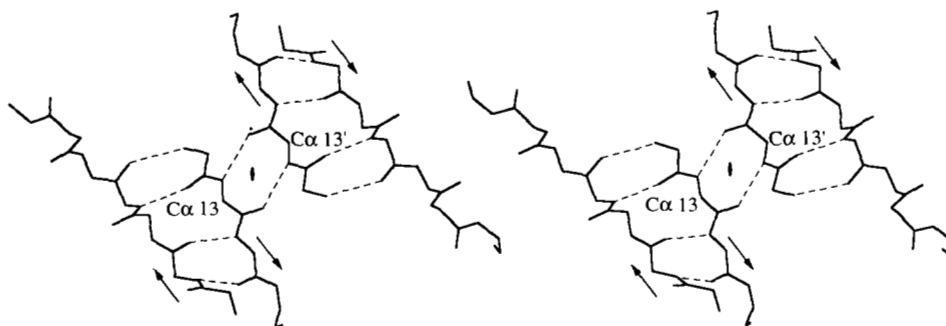

Fig. 7. Stereo figure of part of the β-sheet formed by 2 monomers related by noncrystallographic 2-fold symmetry in the asymmetric unit of monomeric DT crystals. Non-hydrogen main-chain atoms of residues 12–15 and 88–94 are shown; a β-strand formed by residues 133–139 (not shown) is also in the β-sheet. Hydrogen bonds are indicated by broken lines and the direction of the polypeptide chain (N to C) by arrows. The oval symbol represents the noncrystallographic 2-fold axis perpendicular to the plane of the page. Residue 13 in each of the 2 monomers in the asymmetric unit (denoted residues 13 and 13′) forms 2 half hydrogen bonds across the noncrystallographic 2-fold axis.

Table 3. *Hydrogen bonds and salt bridges formed by 2 DT monomers in the asymmetric unit with neighboring molecules in the crystal*

Atom 1		Atom 2[a]		Symmetry relation[b]	Distance[c] (Å)
Monomer 1					
Glu 70[d]	OE2	Arg 407	NH1	I	2.9
Glu 70	OE1	Arg 407	NH2	I	2.9
Glu 70	OE1	Lys 534	NZ	I	3.4
Arg 173	NH2	Lys 385	O	I	3.2
Ala 294	O	Gln 387	NE2	I	3.3
Tyr 358	OH	His 384	O	I	2.8
Asn 359	N	Gln 387	OE1	I	2.8
Asp 519	OD2	Lys 445'	NZ	III	3.3
Asn 524	N	Asp 465'	OD1	III	2.9
Monomer 2					
Glu 15'	OE2	Asn 228'	ND2	II	3.1
Lys 39'	NZ	Glu 256	OE1	II	3.7
Glu 70'	OE2	Arg 407'	NH1	I	3.2
Glu 70'	OE1	Arg 407'	NH2	I	3.2
Glu 70'	OE2	Lys 534'	NZ	I	4.0
Arg 173'	NH2	Lys 385'	O	I	3.5
Ala 294'	O	Gln 387'	NE2	I	3.0
Tyr 358'	OH	His 384'	O	I	2.6
Asn 359'	N	Gln 387'	OE1	I	2.9
Asp 519'	OD2	Lys 445	NZ	III	3.0
Asp 519'	OD1	Lys 445	NZ	III	3.2
Asn 524'	N	Asp 465	OD1	III	2.8

[a] Atom 2 is in a symmetry-related molecule.

[b] Symmetry operators for the space group $P2_12_12$ relating atom 2 to the corresponding atom in the reference molecule are: I, unit translation along c; II, 2-fold screw axis along b at $a = 1/4$, $c = 0$; III, 2-fold screw axis along a at $b = 1/4$, $c = 0$.

[c] Distance between hydrogen bond donor and acceptor atoms. Includes all salt bridges ≤ 4.0 Å and hydrogen bonds ≤ 3.5 Å.

[d] The molecule placed in the unit cell by molecular replacement (see Materials and methods) is numbered 1–535; the molecule related by noncrystallographic symmetry is numbered 1'–535'.

same residues in monomer 1 and Asn 228' forms an intermolecular hydrogen bond, which is not present in monomer 1. In general, residues in intermolecular contacts in monomeric DT also have lower *B* factors than the same residues in dimeric DT.

Discussion

Structure-based mechanism of intoxication

Each domain of DT performs an essential function in pathogenesis: the T and R domains are the machinery for delivering an enzyme, the C domain, to the cytosol. Because it performs a catalytic, rather than stoichiometric role, a single C domain is able to inactivate many EF-2 molecules. Statistical methods have shown that a single C domain can kill a cell in only 2 days (Yamaizumi et al., 1978). Taken together, the structures of monomeric and dimeric DT suggest the outlines of a structure-based mechanism of intoxication as shown in Figure 8.

1. *Proteolysis.* A disulfide-linked loop of 16 residues connects the C and T domains (residues 186–201). This loop is flexible and is disordered in our crystals and is proteolyzed at 1 of 3 Arg

residues (Moskaug et al., 1989) after secretion of DT by *C. diphtheriae* (Fig. 8, panel 1). Proteolysis allows the C domain to dissociate from the T and R domains once the disulfide bridge between residues 186 and 201 is reduced. Disulfide reduction takes place within the intoxicated cell, perhaps as the C domain is translocated to the cytoplasm (Papini et al., 1993).

2. *Receptor binding.* A β-hairpin loop protruding from the R domain (residues 514–525) (discussed above) is likely to be involved when DT binds the cell-surface DT receptor (Fig. 8, panel 2). This hypothesis is supported by a study that finds residue Ser 525 (Greenfield et al., 1987) necessary for receptor binding. Once DT binds the receptor, the DT–receptor complex undergoes receptor-mediated endocytosis (Morris et al., 1985). The receptor for DT has been cloned (Naglich et al., 1992) and its predicted amino acid sequence found virtually identical to that of heparin-binding epidermal growth factor (HB-EGF) precursor (Higashiyama et al., 1991), showing that DT opportunistically uses as a receptor a cell-surface molecule, which has another function. The DT receptor is predicted to be a 185-amino acid protein with an amino-terminal extracellular domain, single transmembrane helix, and carboxy-terminal cytoplasmic domain (Naglich et al., 1992). The cytoplasmic domain contains 2 tyrosines that may be involved in receptor-mediated endocytosis and the transmembrane domain contains an unpaired cysteine that may be involved in reducing the disulfide bond between the C and T domains (Naglich et al., 1992).

3. *Open monomer formation and membrane insertion.* Based on the refined DT structures and hydrophobicity analysis, we suggest 4 potential transmembrane helices in the T domain as shown in Figure 8, panel 3 (A, residues 269–289; B, residues 301–321; C, residues 328–348; and D, residues 351–371) (Bennett et al., 1994b). These helices do not correspond exactly to helices in the T domain (Fig. 3) but are essentially helices TH5, 6–7, 8, and most of 9. Pairs of these helices, A and B, and C and D, are linked by loops containing 4 and 2 acidic residues, respectively. These acidic residues were previously referred to as the "dagger-tips" (Choe et al., 1992) and are represented in Figure 8, panel 3, as protonated carboxylate groups in the loops between A and B, and C and D. At low pH, protonation of these residues might allow the loops to lead the penetration of the pairs of transmembrane helices through the endosomal membrane. The mutation of Glu 349 to Lys in the C–D loop impairs the DT cytotoxicity by reducing low pH-triggered translocation across membranes (O'Keefe et al., 1992), supporting the hypothesis that protonation of acidic residues in the T domain is involved in membrane insertion and subsequent translocation.

In addition, an open monomer structure may form within the low pH of the endosome, where we would expect the noncovalent interactions between the C and R domains are weakened. Specifically, 3 salt bridges between the C and R domains (Asp 47–His 492, Asp 97–Lys 447, and Glu 148–Lys 456) are presumably weakened by protonation as the pH drops. This could lead to noncovalent dissociation of the R domain from the C and T domains and formation of an open monomer structure, perhaps similar to the structure of the open monomer within dimeric DT (Bennett et al., 1994b) (Fig. 8, panel 3). Forming the open monomer requires about 16 kcal/mol in hydrophobic folding energy, as calculated from atomic solvation parameters (Eisenberg & McLachlan, 1986), because of the exposure of apolar residues in the T and R domains. Two of the potential transmembrane helices contain apolar segments that become exposed in the open
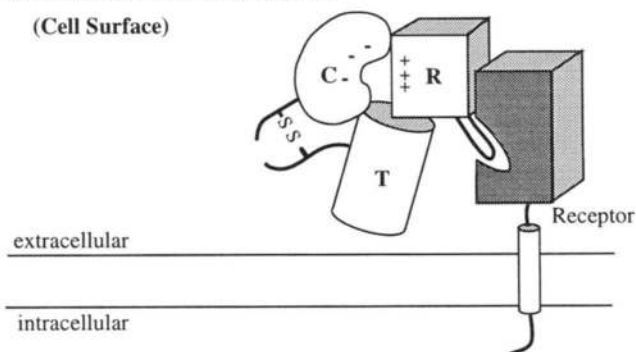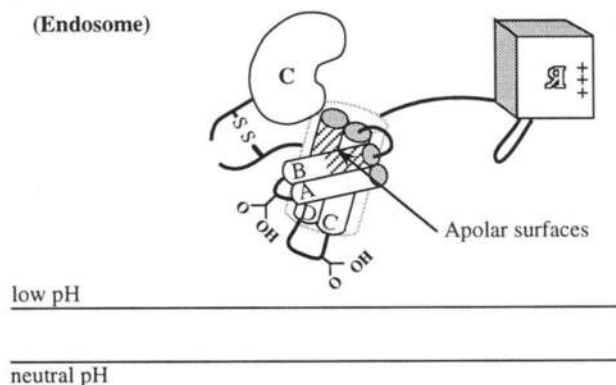
1. PROTEOLYSIS
(Cell Surface)
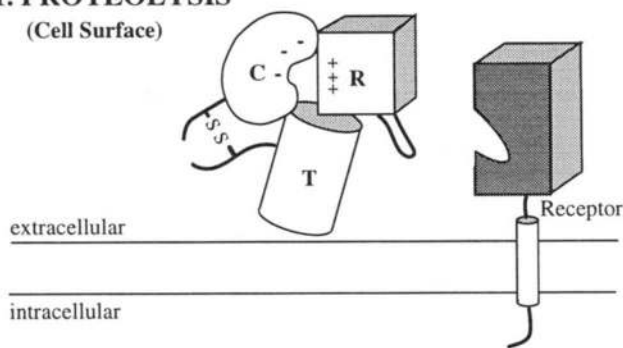
2. RECEPTOR BINDING
(Cell Surface)

3. OPEN MONOMER
(Endosome)

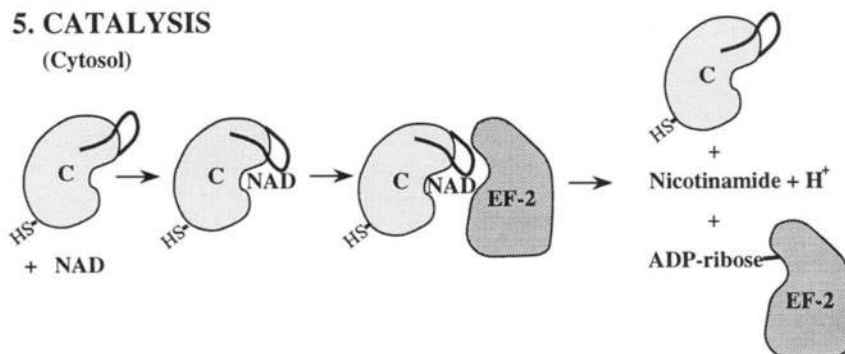## 4. TRANSLOCATION

?

5. CATALYSIS
(Cytosol)

Fig. 8. The proposed structure-based mechanism of intoxication by DT shown schematically. The 3 domains of the DT molecule are labeled C (catalytic, residues 1–190), T (transmembrane, residues 191–378), and R (receptor-binding, residues 379–535). Panel 1: Proteolysis of the disulfide-linked surface loop (residues 186–201) allows the C domain to dissociate from the T and R domains when the disulfide bond between residues 186 and 201 is reduced in the cell. Three salt bridges between the C and R domains (Asp 47–His 492, Asp 97–Lys 447, Glu 148–Lys 456) are indicated by the symbols − and +, representing acidic and basic residues, respectively. Panel 2: Receptor binding by a β-hairpin loop (residues 514–525) shown protruding from the surface of the R domain. Panel 3: Open monomer formation triggered by low pH. Protonation of acidic residues in the C domain probably weakens 3 salt bridges between the C and R domains. Four potential transmembrane helices are represented as cylinders and labeled A (residues 269–289), B (residues 301–321), C (residues 328–348), and D (residues 351–371). The open monomer exposes apolar surfaces on helices B and D, indicated as striped patches. Acidic resides (Asp 290, Glu 292, Asp 295, Glu 298, Glu 349, and Asp 352) in the loops between helices A and B and helices C and D are represented as protonated carboxylate groups. Panel 4: The molecular mechanism of translocation remains obscure (see text). Panel 5: The toxic reaction involves the sequential binding of substrates. NAD binds first and may cause a conformational change in a loop covering the active-site cleft (residues 34–52), which allows EF-2 to bind. After the transfer of ADP-ribose to EF-2 (inactivating EF-2), the C domain undergoes subsequent rounds of catalysis.

monomer (residues 306–311 and 316–319 in helix B, and residues 367–371 in helix D). These apolar segments are represented in Figure 8, panel 3, as striped patches.

4. *Translocation.* The C domain is translocated across the endosomal membrane. It is not known whether more than 1 DT molecule is required to translocate the C domain. It has been shown that residues 322–382 in the T domain (corresponding to the proposed transmembrane helices C and D) form ion channels in lipid bilayer membranes (Silverman et al., 1994). These ion channels have properties identical to channels formed by whole toxin, suggesting that helices C and D are a minimal channel-forming domain. However, the minimum translocation domain remains obscure. As discussed above, we have identified 4 potential transmembrane helices, which are too few to form a pore. Rather than forming a pore, helices from the T domain of a single DT molecule might instead shield polar segments in the C domain as it traverses the membrane. Hydrophobic photolabeling experiments have shown that the C domain interacts with the hydrocarbon chains of photoreactive phospholipids in liposomes (Montecucco et al., 1985), supporting the hypothesis that the C domain contacts the membrane as it is translocated. In addition, the C domain undergoes a conformational change in low pH, becoming hydrophobic, exposing buried tryptophan residues, and interacting with lipid vesicles (Zhao & London, 1988). This conformational change is reversible, consistent with the possibility that the C domain unfolds to cross the membrane, partially shielded by the T domain, then refolds in the cytosol.

5. *Catalysis.* In the cytosol, the C domain catalyzes the transfer of ADP-ribose from NAD to EF-2, thus inactivating EF-2 and halting protein synthesis, which results in cell death (Collier, 1975). The reaction proceeds with sequential binding of substrates, first of NAD, then of EF-2 (Chung & Collier, 1977). The DT structures suggest a reason for sequential binding: a long loop in the C domain (residues 34–52) covers the active-site cleft and may be involved in binding NAD (Bennett et al., 1994b). A change in loop conformation upon NAD binding may be a prerequisite for EF-2 binding (Fig. 8, panel 5). The DT structure also suggests why whole DT cannot catalyze the toxic reaction (Collier, 1975): entry to the active site is blocked in whole DT by the R domain.

In summary, the structure of monomeric DT and its comparison to the structure of dimeric DT yield the beginnings of a structure-based description of the many actions of DT in its pathogenesis.

Materials and methods

Purification and crystal growth by seeding

Partially purified uncleaved DT was purchased from Connaught Laboratories (Willowdale, Ontario, Canada), incubated with a 2-fold molar excess of the inhibitor ApUp and further purified following the method of Carroll et al. (1986b).

Monomeric DT crystals were grown using both microseeding and macroseeding in conditions similar to the preliminary crystallization conditions described by Collier et al. (1982). Crystals were grown in 17% (w/v) polyethylene glycol (PEG) 8000, 1.0 M NaCl, 0.05 M Tris-HCl, pH 7.5, using hanging drop vapor diffusion at 25 °C. Initial crystals were grown in 10-μL hanging drops from a protein concentration of 17 mg/mL. Initial crystals were small, twinned needles and therefore not suited to

X-ray diffraction analysis. Microseeds were obtained from these crystals using a rabbit whisker (Stura & Wilson, 1991) and introduced into hanging drops having the same volume and precipitant composition as the initial drops, but having a protein concentration of only 8 mg/mL. These drops were equilibrated 3 days before seeding. Crystals grew from microseeds within several hours and reached maximum size after 3 days. Crystals grown from microseeds had greatly improved morphology (clean edges and single crystals) but were too small for data collection ($0.05 \times 0.05 \times 0.2$ mm^3). To increase crystal size, single crystals were washed in 2/3 strength mother liquor (11.2% [w/v] PEG 8000, 0.7 M NaCl, 0.03 M Tris-HCl, pH 7.5) and introduced as macroseeds into hanging drops, which were identical to those used for microseeding (Fig. 9A). Crystal size increased dramatically overnight (Fig. 9B) and continued to increase for several days, with several hundred-fold increases in crystal volume (final size $0.5 \times 0.25 \times 1.3$ mm^3).

Monomeric DT crystals belong to space group $P2_12_12$ with unit cell edges $a = 173.4$ Å, $b = 142.3$ Å, and $c = 47.5$ Å. Crystal density was analyzed using aqueous Ficoll solutions (Westbrook, 1985), which showed there are 2 molecules in the asymmetric unit, giving a Matthews number (Matthews, 1968) of 2.5 Å^3/Da. This is in contrast to the initial characterization
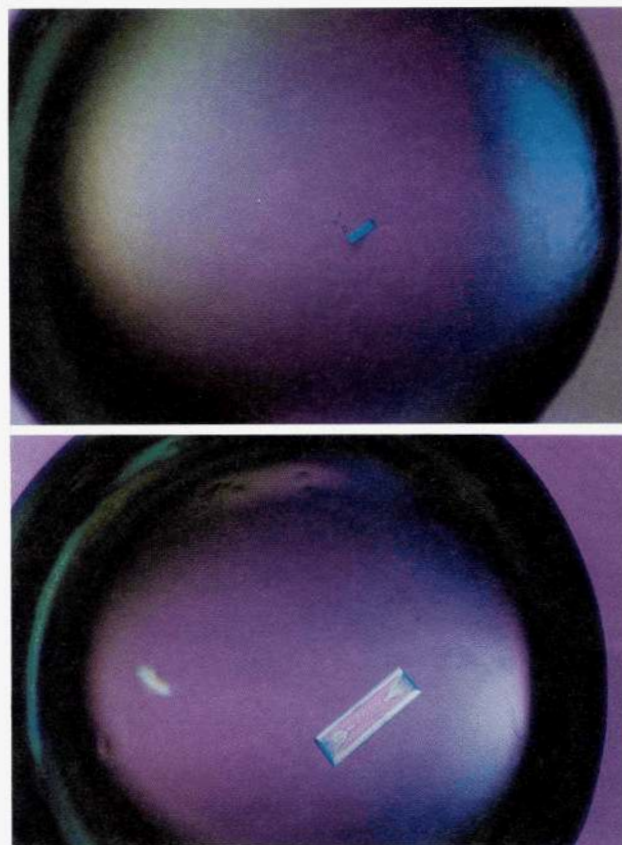

Fig. 9. Monomeric DT crystals. **A:** Monomeric DT crystal macroseed immediately after transfer into a new crystal growth drop. Length in the 2 visible dimensions, corresponding to the **a** and **c** axes: 0.04 mm and 0.16 mm, respectively. **B:** The same monomeric DT crystal as in A, dramatically increased in size after 24 h. Length in the 2 visible dimensions, corresponding to the **a** and **c** axes: 0.19 mm and 0.60 mm, respectively.

of this crystal form, which suggested there was only 1 molecule in the asymmetric unit (Collier et al., 1982).

For X-ray data collection at −150 °C, crystals were soaked in a glycerol-containing mother liquor. Although we attempted to stabilize the crystals by raising the PEG concentration and by increasing the glycerol content gradually, they frequently cracked or dissolved. Crystals were gradually transferred (increasing the glycerol content by 2–3%) to sitting drops containing 100 μL of artificial mother liquor (final concentration 25% PEG 8000, 1.0 M NaCl, 0.05 M Hepes, pH 7.5, 11.3% [v/v] glycerol) and soaked for 4–5 h. Crystals that survived soaking were mounted in hair loops using the modified method of Teng (1990) directly from the soaking solution. Upon freezing, the unit cell edges decreased to $a = 168.5$ Å, $b = 135.5$ Å, $c = 47.0$ Å.

X-ray data collection

After mounting, crystals were flash frozen and continuously cooled in a nitrogen gas stream using an open flow cryostat (Molecular Structure Corporation). Data to 2.7 Å resolution were collected at −150 °C from a single crystal of monomeric DT, using 30-min exposures and 1° oscillation steps. The merged data set at 2.7 Å resolution consisted of 26,603 unique reflections with R_{merge} of 8.8%. The data were 88.3% complete to 2.7 Å resolution. For model refinement, data to 2.3 Å resolution were collected from 2 crystals, using 30–60-min exposures and 0.9–1° oscillation steps. The merged data set at 2.3 Å resolution consisted of 44,070 unique reflections with R_{merge} of 7.4%. The data were 89.9% complete to 2.3 Å resolution. All data were collected using an RAXIS II imaging plate (Rigaku) and were integrated and scaled using the RAXIS-II data processing software.

Molecular replacement using the dimeric DT model

Molecular replacement was initiated using the data set at 2.7 Å resolution and a partially refined dimeric DT model. This model contains all 535 residues and consists of a closed monomer. Molecular replacement was done using the programs in XPLOR (Brünger et al., 1990). The cross rotation function, using data in the resolution range 15–4.0 Å and a maximum vector length of 45 Å, gave a top solution (Eulerian angles $\theta_1 = 239.7°$, $\theta_2 = 56.0°$, $\theta_3 = 304.4°$) after Patterson correlation refinement with a corresponding correlation coefficient of 0.117, which was 4.2 times higher than the next highest solution. The translation function using data in the resolution range 15–4.0 Å had a top solution of 12σ above the mean with fractional coordinates (0.206, 0.200, 0.125) and a second highest solution of 10σ above the mean with fractional coordinates (0.106, 0.700, 0.125).

The 2 translation function solutions are consistent with the 2 molecules in the asymmetric unit being related by a noncrystallographic 2-fold axis parallel to the crystallographic 2-fold screw axis along b. This relationship between the 2 molecules in the asymmetric unit was independently determined from the $v = 1/2$ section of the native Patterson map, which has a peak at $u = 0.1$, $w = 0$. The noncrystallographic 2-fold axis is located at approximately $x = 0.2$, $z = 0$.

Refinement of the atomic model to X-ray data

Refinement was initiated using the 2.3-Å-resolution data set and the dimeric DT model refined at 2.0 Å resolution (Bennett et al.,

1994b). This model lacks 12 residues in a disordered loop (188–199) and consists of an open monomer. Therefore, the coordinates used to initiate refinement consisted of the C and T domains from the dimeric DT model (residues 1–378), and the R domain related by 2-fold crystallographic symmetry in the dimer crystals (residues 386–535), with the intervening loop (residues 379–385) omitted. All refinement was performed using the programs in XPLOR (Brünger et al., 1990). The dimeric DT coordinates were first transformed to the monomeric DT unit cell using a matrix determined from preliminary monomeric DT coordinates obtained by molecular replacement and several cycles of simulated annealing refinement against the 2.7-Å data set. The transformed coordinates were refined against the 2.3-Å data set for 20 cycles at 3.0 Å, with the entire molecule modeled as a rigid body, invoking strict noncrystallographic symmetry. A typical refinement cycle consisted of positional, simulated annealing, and restrained individual isotropic B factor refinements; 42,844 reflections ($F > 1\sigma(F)$) between 10 and 2.3 Å were used for refinement. After the first cycle of refinement, the crystallographic R factor was 28.6%.

Little manual rebuilding of the model was necessary, except for segments that differ in monomeric and dimeric DT, because *the coordinates had been extensively rebuilt and refined against the dimeric DT X-ray data at 2.0 Å resolution*. The 2 longest such segments consisted of the hinge loop, which changes conformation upon dimerization (residues 379–386), and a loop that had to be rebuilt because of differences in the intermolecular contacts in monomeric DT crystals (residues 408–411). In the first 2 cycles of rebuilding and refinement, residues 379–385 were built into what was essentially an unbiased omit map (because these residues had never been included in the model, there was no model bias in this region of the electron density map). The *polypeptide chain trace for the segment 379–386 was clear in the electron density*, including density for the large side chains of Tyr 380 and His 384. Adding residues 379–386, rebuilding residues 408–411, and including 71 water molecules reduced the crystallographic R factor to 26.0%.

A measure of the precision of the refinement is offered by the 2 independent DT monomers in the asymmetric unit. Strict noncrystallographic symmetry constraints were imposed for the first 4 cycles of refinement, noncrystallographic symmetry restraints for 1 cycle, and no restraints for the final 7 cycles. As shown in Figure 1, the RMS differences between the 2 monomers in the asymmetric unit are small (0.4 Å, based on all Cα atoms), with the exception of 5 residues in 2 surface loops, one of which (residues 350–353) is modeled differently in the 2 monomers. The noncrystallographic symmetry is also preserved for 119 of the modeled waters, for which the overall RMS difference is 0.5 Å.

Acknowledgments

References

Bennett MJ, Choe S, Eisenberg D. 1994a. Domain swapping: Entangling alliances between proteins. *Proc Natl Acad Sci USA 91*:3127–3131.
Bennett MJ, Choe S, Eisenberg D. 1994b. Refined structure of dimeric diphtheria toxin at 2.0 Å resolution. *Protein Sci 3*:1444–1463.

Bowie JU, Luethy R, Eisenberg D. 1991. A method to identify protein sequences that fold into a known three-dimensional structure. *Science* 253:164–170.

Brünger AT, Krukowski A, Erickson JW. 1990. Slow cooling protocols for crystallographic refinement by simulated annealing. *Acta Crystallogr A* 46:585–593.

Carroll SF, Barbieri JT, Collier RJ. 1986a. Dimeric form of diphtheria toxin: Purification and characterization. *Biochemistry 25*:2425–2430.

Carroll SF, Barbieri JT, Collier RJ. 1986b. Diphtheria toxin: Purification and properties. *Methods Enzymol 165*:68–76.

Choe S, Bennett MJ, Fujii G, Curmi PMG, Kantardjieff KA, Collier RJ, Eisenberg D. 1992. The crystal structure of diphtheria toxin. *Nature* 357:216–222.

Chung DW, Collier RJ. 1977. The mechanism of ADP-ribosylation of elongation factor 2 catalyzed by fragment A from diphtheria toxin. *Biochim Biophys Acta 483*:248–257.

Collier RJ. 1975. Diphtheria toxin: Mode of action and structure. *Bacteriol Rev 39*:54–85.

Collier RJ, Westbrook EM, McKay DB, Eisenberg D. 1982. X-ray grade crystals of diphtheria toxin. *J Biol Chem 257*:5283–5285.

Eisenberg D, McLachlan AD. 1986. Solvation energy in protein folding and binding. *Nature 319*:199–203.

Freeman VJ. 1951. Studies on the virulence of bacteriophage-infected strains of *Corynebacterium diphtheriae. J Bacteriol 61*:675–688.

Greenfield L, Bjorn MJ, Horn G, Fong D, Buck GA, Collier RJ, Kaplan DA. 1983. Nucleotide sequence of the structural gene for diphtheria toxin carried by corynephage β. *Proc Natl Acad Sci USA 80*:6853–6857.

Greenfield L, Johnson VG, Youle RJ. 1987. Mutations in diphtheria toxin separate binding from entry and amplify immunotoxin selectivity. *Science 238*:536–539.

Higashiyama S, Lau K, Besner GE, Abraham JA, Klagsbrun M. 1991. Structure of heparin-binding EGF-like growth factor. *J Biol Chem 267*: 6205–6212.

Janin J, Miller S, Chothia C. 1988. Surface, subunit interfaces and interior of oligomeric proteins. *J Mol Biol 204*:155–164.

Kabsch W. 1978. A discussion of the solution for the best rotation to relate two sets of vectors. *Acta Crystallogr A 34*:827–828.

Kabsch W, Sander C. 1983. Dictionary of protein secondary structure: Pattern recognition of hydrogen-bonded and geometrical features. *Biopolymers 22*:2577–2637.

London E. 1992. Diphtheria toxin: Membrane interaction and membrane translocation. *Biochim Biophys Acta 1113*:25–51.

Matthews BW. 1968. Solvent content of protein crystals. *J Mol Biol 33*:491–497.

Montecucco C, Schiavo G, Tomasi M. 1985. pH-dependence of the phospholipid interaction of diphtheria-toxin fragments. *Biochem J 231*:123–128.

Morris RE, Gerstein AS, Bonventre PF, Saelinger CB. 1985. Receptor-mediated entry of diphtheria toxin into monkey kidney (Vero) cells: Electron microscopic evaluation. *Infect Immunol 50*:721–727.

Moskaug JO, Sletten K, Sandvig K, Olsnes S. 1989. Translocation of diphtheria toxin A-fragment to the cytosol. *J Biol Chem 264*:15709–15713.

Naglich JG, Metherall JE, Russel DW, Eidels L. 1992. Expression cloning of a diphtheria toxin receptor: Identity with a heparin-binding EGF-like growth factor precursor. *Cell 69*:1051–1061.

O'Keefe DO, Cabiaux V, Choe S, Eisenberg D, Collier RJ. 1992. pH-dependent insertion of proteins into membranes: B chain mutation of diphtheria toxin that inhibits membrane translocation, Glu 349-Lys. *Proc Natl Acad Sci USA 89*:6202–6206.

Papini E, Rappuoli R, Murgia M, Montecucco M. 1993. Cell penetration of diphtheria toxin: Reduction of the interchain disulfide bridge is the rate-limiting step of translocation in the cytosol. *J Biol Chem 268*:1567–1574.

Richardson JS. 1981. The anatomy and taxonomy of protein structure. *Adv Protein Chem 34*:167–338.

Richmond TJ, Richards FM. 1978. Packing of α-helices: Geometrical constraints and contact areas. *J Mol Biol 119*:537–555.

Silverman JA, Mindell JA, Zhan H, Finkelstein A, Collier RJ. 1994. Structure–function relationships in diphtheria toxin channels: I. Determining a minimum channel-forming domain. *J Membr Biol 137*:17–28.

Stura EA, Wilson IA. 1991. Applications of the streak seeding technique in protein crystallization. *J Crystal Growth 110*:270–282.

Teng TY. 1990. Mounting of crystals for macromolecular crystallography in a free-standing thin film. *J Appl Crystallogr 23*:387–391.

Westbrook EM. 1985. Crystal density measurements using aqueous Ficoll solutions. *Methods Enzymol 114*:187–196.

Yamaizumi M, Mekada E, Uchida T, Okada Y. 1978. One molecule of diphtheria toxin fragment A introduced into a cell can kill the cell. *Cell 15*: 245–250.

Zhang KYJ, Eisenberg D. 1994. The 3D profile method using residue preference as a continuous function of its environments. *Protein Sci 3*:687–695.

Zhao JM, London E. 1988. Conformation and model membrane interactions of diphtheria toxin fragment A. *J Biol Chem 263*:15369–15377.